Physics – Uspekhi **55** (9) 929 – 941 (2012)

CONFERENCES AND SYMPOSIA PACS numbers: 01.10.Fv, **26.60. – c**, **52.35. – g**, **67.10. – j**, **96.60. – j**, 97.10.Sj, 97.60.Jd

Challenges in astrophysics
(Scientific session of the Physical Sciences Division of the Russian Academy of Sciences, 25 January 2012)

DOI: 10.3367/UFNe.0182.201209e.0999

On 25 January 2012, the scientific session of the Physical Sciences Division of the Russian Academy of Sciences (RAS), entitled as ''Challenges in astrophysics'', was held at the conference hall of the Lebedev Physical Institute, RAS.

The following reports were put on the session agenda posted on the website www.gpad.ac.ru of the RAS Physical Sciences Division:

(1) **Stepanov A V** (Central (Pulkovo) Astronomical Observatory, RAS, St. Petersburg) ''Coronal seismology'';

(2) **Yakovlev D G** (Ioffe Physical Technical Institute, St. Petersburg; St. Petersburg State Polytechnical University, St. Petersburg) ''Superfluid neutron stars''.

The papers written on the base of the oral reports are published below.

PACS numbers: **52.35. – g**, **96.60. – j**, 97.10.Sj
DOI: 10.3367/UFNe.0182.201209f.0999

Coronal seismology

A V Stepanov, V V Zaitsev, V M Nakariakov

1. Introduction

Coronal seismology is a new, rapidly developing branch of astrophysics studying wave and oscillatory phenomena intrinsic to coronae of active stars. The idea of coronal seismology is reminiscent of that of *geoseismology* and lies in the remote sensing of coronal plasma parameters. In solar and stellar physics, a similar approach is applied in *helio-* and *asteroseismology*. Present-day observations of waves and oscillations in accretion disks led to the appearance of *diskoseismology*.

The task of helioseismology consists in testing and perfecting the model of the Sun. Among its achievements is the confirmation of the 'standard' Sun model and the creation of the shallow sunspot model [1]. Newly emerging tasks of helioseismology are being solved with the help of the operating NASA's Solar Dynamic Observatory (SDO) mission [2]. The main tasks of asteroseismology concern the verification and improvement of existing evolutionary models of stars.

The founders of *coronal seismology* are Y Uchida [3], who proposed exploring the plasma of the Sun's corona with the help of oscillations and waves, and H Rosenberg [4], who explained pulsations in solar radio-frequency emission by magnetohydrodynamic (MHD) oscillations in its source. Observations of solar ultraviolet (UV) emission in space by the NASA's TRACE (Transition Region and Coronal Explorer) mission revealed oscillations of coronal loops [5] (Fig. 1), which gave impetus to the fast development of coronal seismology.

The magnetic structure of the coronae of the Sun and other stars includes both open and closed configurations (magnetic tubes). Solar spicules, jets, and streamers are the examples of open configurations. Among the closed configurations are flaring active regions consisting of a system of loops, seldom of a single loop flare. Flare loops make up magnetic traps for accelerated particles. MHD oscillations of loops are accompanied by variations in the magnetic field and gas pressure, as well as by the modulation of high-energy particle fluxes to the loop footpoints. For this reason, the flare emission is modulated in a broad band, including radio, optical, X-ray, and gamma ranges. Characteristics of these modulations are used to diagnose flare parameters.

Two approaches are routinely used to describe wave and oscillatory phenomena in stellar coronae. In the first one, coronal magnetic loops and tubes are considered as resonators and waveguides for MHD oscillations and waves. In the second approach, the coronal magnetic loop is viewed as an electric current circuit. Both approaches are indispensable for diagnosing physical processes in stellar coronae.

2. Coronal resonators and waveguides

The impedance for MHD waves experiences a jump at the boundary between coronal loops and the ambient medium; hence, a coronal loop can be conceived of as a resonator. In the first approximation, loop oscillations can be explored by considering a homogeneous plasma cylinder of radius a and length l, the ends of which are frozen in a highly conductive plasma. The plasma inside the cylinder has the density ρ_i, temperature T_i, and magnetic field induction B_i along the cylinder axis. The respective parameters outside the cylinder are ρ_e, T_e, and B_e. The dispersion relation connecting the

A V Stepanov Central (Pulkovo) Astronomical Observatory, Russian Academy of Sciences, St. Petersburg, Russian Federation
E-mail: stepanov@gao.spb.ru
V V Zaitsev Institute of Applied Physics, Russian Academy of Sciences, Nizhny Novgorod, Russian Federation
E-mail: za130@appl.sci-nnov.ru
V M Nakariakov Centre for Fusion, Space, and Astrophysics, Physics Department, University of Warwick, Coventry CV4 7AL, UK
E-mail: V.Nakariakov@warwick.ac.uk

Uspekhi Fizicheskikh Nauk **182** (9) 999 – 1012 (2012)
DOI: 10.3367/UFNr.0182.201209e.0999
Translated by S D Danilov, D G Yakovlev; edited by A Radzig

Uspekhi Fizicheskikh Nauk **182** (9) 999 – 1005 (2012)
DOI: 10.3367/UFNr.0182.201209f.0999
Translated by S D Danilov; edited by A Radzig

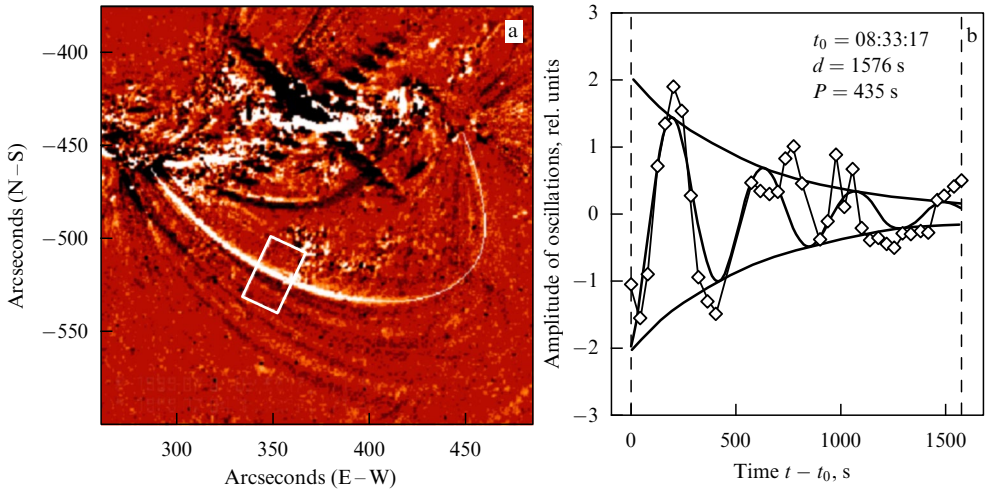

Figure 1. (a) An example of oscillations of the coronal loop for the flare on July 4, 1999, recorded by space mission TRACE in the 171 Å line. (b) Their approximation by exponentially decaying periodic oscillations. The period of pulsations $P = 435$ s, their duration $d = 1576$ s, and their amplitude was on the order of 700 km [5].

frequency ω of natural oscillations of the cylinder with the wave vector components $k_\perp$ and $k_\parallel$ takes the form [6, 7]

$$\frac{J'_m(\kappa_i a)}{J_m(\kappa_i a)} = \alpha \frac{H_m^{(1)'}(\kappa_e a)}{H_m^{(1)}(\kappa_e a)} . \qquad (1)$$

Here, the following notations were introduced:

$$\kappa^2 = \frac{\omega^4}{\omega^2(c_s^2 + c_A^2) - k_\parallel^2 c_s^2 c_A^2} - k_\parallel^2 , \qquad \alpha = \frac{\kappa_e \rho_i}{\kappa_i \rho_e} \frac{\omega^2 - k_\parallel^2 c_{Ai}^2}{\omega^2 - k_\parallel^2 c_{Ae}^2} ,$$

c_s is the speed of sound, c_A is the Alfvén speed, J_m and $H_m^{(1)}$ are the Bessel function and the Hankel function of the first kind, respectively, and $k_\parallel = \pi s/l$, $s = 1, 2, 3, \ldots$. For a thin $(a/l \ll 1)$ and dense $(\rho_e/\rho_i \ll 1)$ cylinder, we find the frequency of fast (FMA) and slow (SMA) magneto-acoustic oscillations from Eqn (1) at $m = 0$:

$$\omega_f = (k_\perp^2 + k_\parallel^2)^{1/2}(c_{si}^2 + c_{Ai}^2)^{1/2} , \qquad \omega_s = \frac{k_\parallel c_{si} c_{Ai}}{(c_{si}^2 + c_{Ai}^2)^{1/2}} . \qquad (2)$$

The transverse wave number $k_\perp = \lambda_j/a$, where λ_j are the zeros of the Bessel function $J_0(\lambda) = 0$.

Radial FMA oscillations (the sausage mode), contributing most to the modulation of loop emission, may experience substantial damping due to their emission into the surrounding medium [8]:

$$\gamma_a = \frac{\pi}{2} \omega_f \left(\frac{\rho_e}{\rho_i} - \frac{k_\parallel^2}{k_\perp^2} \right) , \qquad \frac{\rho_e}{\rho_i} > \frac{k_\parallel^2}{k_\perp^2} . \qquad (3)$$

The mechanism for acoustic damping is apparent: loop oscillations are accompanied by the excitation of waves in the surrounding medium, which requires the oscillation energy expenditure. The acoustic damping is absent for $\rho_e/\rho_i < k_\parallel^2/k_\perp^2$, which corresponds to total internal reflection, i.e., a 'thick' loop with $l/a < 1{,}3(\rho_i/\rho_e)^{1/2}$ is an ideal resonator for FMA waves. Oscillations in the global FMA mode were observed in the solar flare on January 12, 2000, recorded at a frequency of 17 GHz by Radioheliograph Nobeyama [9]. In this case, all regions of the flare loop were oscillating in phase with the period $P \approx l/c_{Ai} \approx 15$ s.

The case of $m = 1$ corresponds to kink loop oscillations (see Fig. 1) which were observed for the first time by TRACE. For $k_\parallel a \ll 1$ and $B_e \approx B_i$, equation (1) yields the kink mode frequency [10]

$$\omega_k \approx k_\parallel \left(\frac{2}{1 + \rho_e/\rho_i} \right)^{1/2} c_{Ai} . \qquad (4)$$

In the event on July 4, 1999 (see Fig. 1), the phase velocity of kink mode approached to $\omega/k_\parallel = 2l/P \approx 1000$ km s^{-1}. Taking into account relation (4) and assuming $\rho_e/\rho_i = 0.1$ in the interval $10^9 - 10^{10}$ cm^{-3} of electron density in the loop, we estimate the magnetic field intensity:

$$B_i = \sqrt{2\pi} \frac{2l}{P} \sqrt{\rho_i \left(1 + \frac{\rho_e}{\rho_i} \right)} \approx 10 - 33 \text{ G} .$$

A numerical solution of the transcendent equation (1) with a complex frequency of oscillations $\omega = \omega_0 - i\gamma$, where γ is the decrement, is plotted in Fig. 2 which shows the dependences of $\omega_0/k_\parallel$ and $\gamma/k_\parallel$ on $k_\parallel a = s\pi a/l$ for the first three harmonics of FMA oscillations [11].

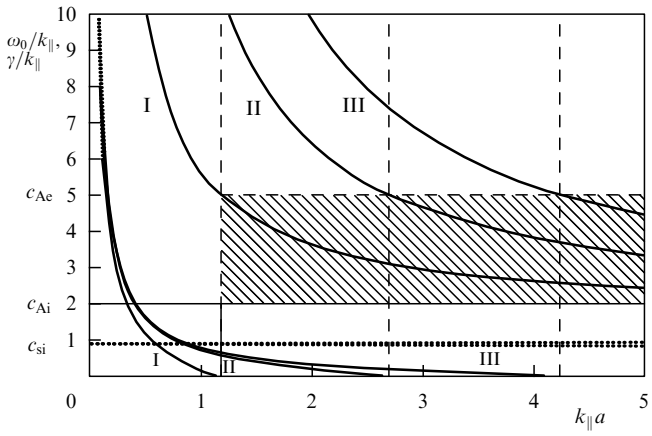

Figure 2. Dispersion curves and decrements of acoustic damping for the first three harmonics of FMA oscillations at $c_{se} = 0.5c_{si}$, $c_{Ai} = 2c_{si}$, and $c_{Ae} = 5c_{si}$ [11].

To compare the results of Ref. [11] to those obtained by Edwin and Roberts [7] for trapped modes, the same relationships as in the latter work have been used for velocities in the solar corona. The dispersion curves in the domain of trapped modes in the interval $c_{Ai} < \omega_0/k_\parallel < c_{Ae}$ (the dashed area in Fig. 2) coincide with those in Ref. [7] and have a natural continuation for $\omega_0/k_\parallel > c_{Ae}$. It was assumed in Ref. [7] that $\kappa_e^2 < 0$, i.e., the arguments of cylindrical functions were taken as imaginary. In this case, the solution of Eqn (1) in the outer domain is expressed in terms of the Mcdonald function $K_m(z) = (\pi/2)\mathrm{i}^{m+1}H_m^{(1)}(\mathrm{i}z)$, i.e., the solution of equation (1) includes nonleaky modes as a particular case for the imaginary $\kappa_e a$. Note that the nonleaky sausage modes occur only for 'thick' loops: $k_\parallel a = s\pi a/l > 1$. In coronae of the Sun (see Fig. 1) and stars the loops are thin: $k_\parallel a < 1$, i.e., the MHD modes are emitting. Simultaneously, the period of FMA oscillations is determined not by the length of the loop, but by its radius:

$$P_f = \frac{2\pi a}{\lambda_j\sqrt{c_{Ai}^2 + c_{si}^2}}\,. \qquad (5)$$

Figure 2 also depicts the branches of the SMA mode $\omega_s = k_\parallel c_{si}$, and the Alfvén mode $\omega_A = k_\parallel c_{Ai}$. Accounting for curvature of the magnetic field in coronal loops is important for the ballooning mode of the flute type instability [12].

In addition to oscillations, one can observe propagating waves (Fig. 3) in coronal loops. The TRACE observations revealed longitudinal compressive waves of a small amplitude (4–10%) with periods of 3–12 min and a mean propagation speed of ≈ 100 km s^{-1} [13]. This interval of periods also includes five-minute photospheric oscillations. The energy flux in these waves of ≈ 0.3 W m^{-2} is, however, substantially lower than the level of order 100 W m^{-2} needed to heat the solar corona to a temperature of 10^6 K.

Incompressible Alfvén type waves are more efficient in carrying the energy of convective motions in stellar photospheres to coronae than are magneto-acoustic waves. It was believed earlier that the amplitudes of Alfvén waves in the solar corona do not exceed 0.5 km s^{-1}, i.e., that their energy flux is insufficient to heat the corona. Recent SDO data [14] have shown that the amplitudes may reach 20 km s^{-1}, i.e., the energy of kink (Alfvénic) waves may suffice to heat the solar corona and accelerate the solar wind. The main problem consists in elucidating the mechanism for kink (Alfvénic) wave dissipation.

MHD modes in X-ray jets and spicules are described with the model of a plasma cylinder with one end fixed [15].

3. Mechanisms of excitation and damping of magnetohydrodynamic oscillations

An often encountered mechanism for the generation of loop oscillations consists in their excitation by an external source, which can be a flare, filament eruption, or electrodynamically coupled neighboring loop-trigger [16]. If flare energy release happens inside a coronal loop, then, given that the flare has a sufficiently fast (impulse) character, the generation of FMA loop oscillations becomes possible [17]. The FMA modes of loops can also be excited by high-energy protons at bounce resonance, $\omega_f = s\Omega$, $s = 1, 2, 3, \ldots$, where Ω is the frequency of oscillations for high-energy protons between magnetic mirrors of the coronal loop. In this case, the pressure of protons trapped in the loop should be fairly high: $\beta_{pr} > 0.2$ [8].

The kink mode (4) can be generated during solar flares and also because of the evaporation of hot ($\geqslant 10^7$ K), dense chromospheric plasma from loop footpoints [18]. The motion of the chromospheric matter at the speed $V \geqslant 3 \times 10^7$ cm s^{-1} along the magnetic field in a loop with the curvature radius R causes the centrifugal force $F_c = \rho V^2/R$ 'stretching' the loop. The tension of magnetic field lines tends to return the loop to its initial state, which results in the excitation of loop oscillations with the period $P_k = 2\pi/\omega_k$. The excitation of loops due to the parametric resonance with acoustic five-minute oscillations of the Sun's photosphere is considered in Section 6.

The Q factor for oscillations in solar and stellar flares is, as a rule, not very high: $Q = \pi\omega/\gamma = 10-30$. Modes without leakage decay because of dissipative processes inside the loops. This, with the exception of special cases, is related to emitting modes, too. The point is that the loop–ambient plasma interface is characterized by an impedance jump for MHD waves and the possible ratio of intensities of incident and reflected waves, $I_{ref}/I_{inc} = (Z_i - Z_e)^2/(Z_i + Z_e)^2$, being close to unity. The impedance for FMA waves is defined as $Z = \rho(c_A^2 + c_s^2)^{1/2}$. If, for example, the ratio $\rho_i/\rho_e \approx 30-100$ and $\beta = 8\pi n k_B T/B^2 \approx (c_s/c_A)^2 \ll 1$, then $I_{ref} \approx I_{inc}$. The total decay decrement for FMA waves, $\gamma_\Sigma = \gamma_J + \gamma_{cond} + \gamma_\nu + \gamma_{rad}$, contains contributions due to Joule dissipation, electron heat conductivity, ion viscosity, and radiation loss [19]:

$$\gamma_J = \frac{1}{2}\frac{m_e}{m_i}\frac{\omega^2}{\omega_i^2}\nu_{ei}\,, \qquad \gamma_{cond} = \frac{1}{3}\frac{m_e}{m_i}\beta^2\frac{\omega^2}{\nu_{ei}}\sin^2\vartheta\cos^2\vartheta\,,$$
$$\gamma_\nu = \frac{1}{12}\sqrt{\frac{m_i}{2m_e}}\left(\frac{V_{Ti}}{c_A}\right)^2\frac{\omega^2}{\nu_{ei}}\sin^2\vartheta\,, \quad \gamma_{rad} = \frac{2\pi}{3}\frac{n^2\phi(T)}{B^2}\sin^2\vartheta\,. \qquad (6)$$

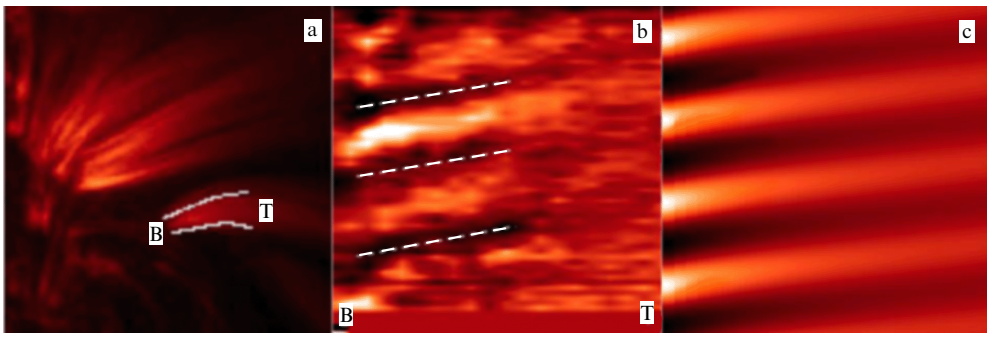

Figure 3. (a) An example of waves propagating from the footpoints of the loop structure as observed by TRACE (171 Å) on April 7, 2000. (b) Time–distance diagram revealing propagating waves. (c) Results of numerical simulations of the propagating perturbation [13].

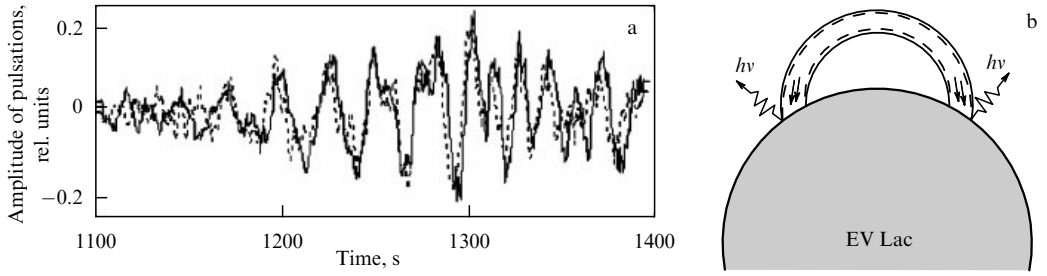

Figure 4. (a) Oscillations of the emission from a flare on EV Lac on 11.09.1998 in the bands U (solid line) and B (dashed line) with the period $P \approx 13$ s [20]. (b) Schematic representation of optical emission pulsations [21].

Here, ϑ is the angle between **B** and the wave vector **k**, ω_i is the ion gyrofrequency, $\nu_{ei} \approx 60nT^{-3/2}\ \mathrm{s}^{-1}$, and $\phi(T) = 5 \times 10^{-20} T^{-1/2}$ is the loss function for the temperature interval $10^6 < T < 10^7$ K [20]. In coronae of the Sun and stars of the UV Ceti type (active red dwarfs) the major contributions to the decay of FMA waves come from electron heat conductivity (γ_{cond}) and ion viscosity (γ_ν). In stellar chromospheres, the main cause of damping is the radiation losses (γ_{rad}).

4. Diagnostics of flare loop parameters

The hypothesis of modulation of the emission from solar and stellar flares with MHD oscillations of loops is successfully invoked to diagnose flare plasmas. In stellar coronae, loop oscillations modulate radio-frequency emission, while in the chromosphere and photosphere they modulate optical, X-ray, and gamma radiations caused by intrusions of high-energy particles in dense footpoints of flare loops. The intensity of emission from the footpoints is proportional to the flux of 'precipitating' accelerated particles, $F \sim l n_1 / \sigma t_D(\sigma)$. Here, n_1 is the number density of high-energy particles, $\sigma = B_{max}/B_{min}$ is the mirror ratio of the loop, and $t_D(\sigma)$ is the pitch-angular particle diffusion time into the loss cone, which depends on the diffusion mode. Relative variations of emitted flux are proportional to the variations of the mirror ratio caused by magnetic field oscillations, i.e., $\delta F/F \approx \delta\sigma/\sigma \approx \delta B/B$. To find δB, we assume that the generation of FMA oscillations proceeds at the expense of the work done by plasma pressure against the loop magnetic field during pulse heating, $\delta p \approx n k_B T$. Consequently, $\delta B/B \approx 4\pi n k_B T/B^2$ and the emission modulation depth is given by [17]

$$\Delta = \frac{\delta F}{F} \approx \frac{4\pi n k_B T}{B^2} = \frac{\beta}{2}\,. \tag{7}$$

From the three equations for the period of FMA oscillations (5) at $\lambda_0 = 2.4$, Q factor $Q = \pi\omega/(\gamma_{cond} + \gamma_\nu)$, and the emission modulation depth (7) we obtain the formulas to determine the parameters of the flare plasma:

$$\begin{aligned} T &\approx 1.2 \times 10^{-8}\, \frac{\tilde{r}^2 \Delta}{P^2 \chi}\ [\mathrm{K}]\,, \\ n &\approx 3.5 \times 10^{-13}\, \frac{\tilde{r}^3 \eta \Delta^{5/2} Q \sin^2\vartheta}{P^4 \chi^{3/2}}\ [\mathrm{cm}^{-3}]\,, \\ B &\approx 3.8 \times 10^{-18}\, \frac{Q^{1/2} \tilde{r}^{5/2} \eta^{1/2} \Delta^{5/4} \sin\vartheta}{P^3 \chi^{5/4}}\ [\mathrm{G}]\,, \end{aligned} \tag{8}$$

where $\tilde{r} = 2\pi a/\lambda_0$, $\eta = 243\beta\cos^2\vartheta + 1$, $\chi = 10\Delta/3 + 1$, and $\vartheta = \arctan(k_\perp/k_\parallel) \approx \arctan(l/a)$.

Let us consider the examples of such diagnostics. Pulsations in the flare on EV Lac 11.09.98 (Fig. 4) were observed in the ultraviolet (UV) and blue (B) bands with a period $P \approx 13$ s, the Q factor ≈ 50, and $\Delta \approx 0.2$ [21]. Setting $a/l = 0.1$, i.e., $\vartheta \approx \arctan(\lambda_0 l/\pi a) \approx 76°$, and assuming $\tilde{r} = 2.62a \approx 2.62 \times 10^9$ cm, from formulas (8) we find $T \approx 3.7 \times 10^7$ K, $n \approx 1.6 \times 10^{11}\ \mathrm{cm}^{-3}$, and $B \approx 320$ G.

For pulsations of the optical emission in the flare on EQPegB (M5e) with a period of about 10 s, the Q factor ≈ 30, and $\Delta \approx 0.1$, from formula (8) we get $T \approx 6 \times 10^7$ K, $n \approx 3 \times 10^{11}\ \mathrm{cm}^{-3}$, and $B \approx 540$ G [22].

A popular method of diagnosing parameters of stellar coronae [23] is based on the assumption that, on plasma cooling, the radiation losses are on the order of losses due to electron heat conductivity: $\gamma_{rad} \approx \gamma_{cond} \approx 1/\tau_d$. Then, based on measurements of the emission measure (EM) and flare decay time τ_d, the temperature, number density, and size of the emitting domain can be determined as:

$$\begin{aligned} T\,[\mathrm{K}] &= 4 \times 10^{-5} (\mathrm{EM})^{0.25} \tau_d^{-0.25}\,, \\ n\,[\mathrm{cm}^{-3}] &= 10^9 (\mathrm{EM})^{0.125} \tau_d^{-0.125}\,, \\ l\,[\mathrm{cm}] &= 5 \times 10^{-6} (\mathrm{EM})^{0.25} \tau_d^{0.75}\,, \end{aligned}$$

and the magnetic field can be estimated from the relationship $\beta < 1$. Our approach allows the estimation of three fundamental parameters, T, n, and B, from the pulsation period, Q factor, and emission modulation depth. Both approaches expand the possibilities of stellar corona diagnostics.

Microwave flare emission is frequently caused by gyrosynchrotron emission of high-energy electrons with a power-law energy spectrum $N(E) \propto E^{-\alpha}$. In this case, the intensity of emission from optically thin and optically thick sources is written down in the form

$$I_\nu \propto \begin{cases} B^{0.9\alpha - 0.22}\,, & \tau_\nu \ll 1\,, \\ B^{-0.52 - 0.08\alpha}\,, & \tau_\nu \gg 1\,. \end{cases} \tag{9}$$

It can easily be seen that the emission of an optically thin source is rather sensitive to magnetic field variations. Moreover, from Eqn (9) it follows that, given appropriate values for α, pulsations of the emission from optically thin and thick sources will be in antiphase, as was observed for the solar flare on May 31, 1990, recorded at frequencies of 9 GHz ($\tau_\nu \gg 1$) and 15 GHz ($\tau_\nu \ll 1$) [24]. The modulation depths for optically thin and thick sources are equal, respectively, to

$$\begin{aligned} \Delta_1(\tau_\nu < 1) &= 2(0.9\alpha - 1.22)\, \frac{\delta B}{B}\,, \\ \Delta_2(\tau_\nu > 1) &= 2(0.08\alpha + 1.02)\, \frac{\delta B}{B}\,. \end{aligned}$$

Thus, one has

$$\alpha = \frac{1.22 + 1.02(\Delta_1/\Delta_2)}{0.9 - 0.08(\Delta_1/\Delta_2)} . \quad (10)$$

For the above-mentioned event, $\Delta_1 = 5\%$, and $\Delta_2 = 2.5\%$. From expression (10) we obtain $\alpha = 4.4$ for the power-law exponent of the high-energy (> 30 keV) electron spectrum. From formulas for gyrosynchrotron emission, one determines the magnetic field induction in the source: $B \approx 150$ G [25].

5. Coronal magnetic loops as equivalent electric (*RLC*) circuits

One of the important problems of coronal physics pertains to diagnosing electric currents. The current in radio source 3C 228 ($I \approx 2.5 \times 10^9$ A) was determined through the rotation of the radiation polarization ellipse (the Faraday effect) [26]. A Severny [27] was the first to estimate the magnitude of current ($I \geqslant 10^{11}$ A) in the vicinity of solar spots based on magnitographic measurements. Based on the measurements by Severny, H Alfvén proposed describing the flare loop in terms of a wire carrying electric current. The Alfvén model [28] gained attention owing to flare loop observations by cosmic solar observatories. The model of the flare as an equivalent electric circuit is described in review [29].

Examples of magnetic tube formation by converging streams of photospheric plasma are given in Fig. 5. There are oppositely directed convective flows across the boundaries separating supergranules, and an extended layer of the magnetic field with relatively substantial strength (Fig. 5a) may appear along the boundaries.

A Rayleigh–Taylor type interchange instability may occur in this layer. As a result, it breaks into a system of magnetic tubes with a radius on the order of the layer thickness (Fig. 5b), which may form an arcade of coronal magnetic loops in the corona. If a magnetic tube made up at a contact point of more than two cells, the converging flow of photospheric plasma forms a compact cylindrical magnetic tube with current from the background magnetic field (Fig. 5c). Indeed, the electron gyrofrequency in the upper photosphere is higher than the effective frequency of electron–atom collisions, $\omega_e \gg \nu'_{ea}$, and the gyrofrequency of ions is lower than the frequency of ion–atom collisions, $\omega_i \ll \nu'_{ia}$. The electrons are, consequently, magnetized, and the ions are entrained by the neutral plasma component, which leads to the emergence of the radial electric field E_r of charge separation. Field E_r, together with the primary magnetic field B_z, generates the Hall current j_φ which amplifies the primary field B_z. The amplification of the magnetic field continues until 'raking' of the background magnetic field is compensated for by magnetic field diffusion. A magnetic tube forms as a result, the magnetic field of which is determined by the energy deposition of the convective plasma flow for the tube formation time of order R_0/V_r, where $R_0 \sim 30{,}000$ km is the scale of the supergranulation cell, and $V_r \sim 0.1$–0.5 km s^{-1} is the horizontal velocity of convective motion.

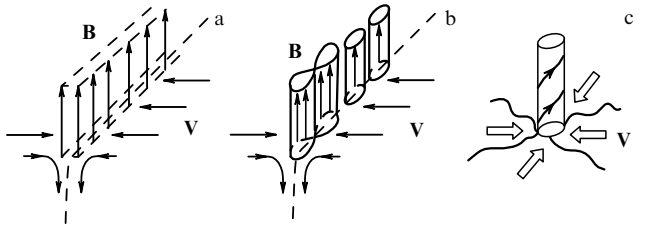

Figure 5. Formation of magnetic field tubes at the boundaries of supergranulation cells: (a) the build-up of the extended thin magnetic layer; (b) breakup of the layer into magnetic tubes as a result of interchange instability, and (c) formation of a magnetic tube in a node of several supergranulation cells.

In the coronal part of the loop, the plasma parameter $\beta \ll 1$ and the loop structure is forceless, i.e., the electric current lines are directed nearly along the magnetic field lines. The current is closed in the subphotospheric domain where the plasma conductivity is isotropic and the current follows the shortest path from one loop footpoint to the other one.

The equation for small-amplitude current oscillations $|\tilde{I}| \ll I$ has the form [30]

$$\frac{L}{c^2}\frac{\mathrm{d}^2\tilde{I}}{\mathrm{d}t^2} + \left[R(I) - \frac{|V_r|l}{ac^2}\right]\frac{\mathrm{d}\tilde{I}}{\mathrm{d}t} + \frac{\tilde{I}}{C(I)} = 0 . \quad (11)$$

Here, the notations are as follows:

$$R(I) \approx \frac{4I^2 l\xi^2}{c^4 n m_i \nu'_{ia}\pi a^4} , \qquad C(I) \approx \frac{c^4 n m_i S^2}{2\pi l I^2} ,$$
$$L = 2l\Lambda , \qquad \Lambda \approx \ln\frac{4l}{\pi a} - \frac{7}{4} , \quad (12)$$

where $\xi = \rho_a/\rho$ is the relative number density of neutral particles, and S is the loop cross-section area. From equation (11) it follows that oscillations in the circuit build up if $R(I) < |V_r|l/ac^2$, i.e., if the current in the circuit is less than the stationary value, and decay if the photospheric electromotive force (EMF) ceases to act. In this case, the decay is rather slow, since the Q factor of the circuit is high: $Q = [cR(I)]^{-1} \times \sqrt{LC(I)} \sim 10^3 - 10^4$ for typical flare loops. From relationships (12) it follows that the frequency of flare-loop *RLC* oscillations for a strong enough current is proportional to its magnitude [29]:

$$\nu_{RLC} = \frac{c}{2\pi\sqrt{LC(I)}} \approx \frac{1}{(2\pi)^{3/2}\Lambda^{1/2}}\frac{I}{ca^2\sqrt{\rho}} \approx \frac{B_\varphi}{2\pi a\sqrt{4\pi\rho}} . \quad (13)$$

The condition that oscillations be in phase requires that relationships for the Alfvén time $\tau_A = l/c_A < T_{RLC} = 1/\nu_{RLC}$ be satisfied. Since $I \approx caB_\varphi/2$, the twisting of the loop magnetic field should be small, $B_\varphi/B_z < \pi\sqrt{2\Lambda}\,(a/l)$, which is observed for solar loops. Formula (13) corresponds to Alfvén oscillations of the coronal magnetic loop with the wave vector of absolute value $|\mathbf{k}| \approx a^{-1}$ directed at the angle $\cos\theta \approx (B_\varphi/B_z)$ to the magnetic field. In this case, one obtains

$$\nu_A = \frac{1}{2\pi} kc_A \cos\theta \approx \frac{1}{2\pi a}\frac{\sqrt{B_z^2 + B_\varphi^2}}{\sqrt{4\pi\rho}}\frac{B_\varphi}{B_z} ,$$

i.e., the frequency of Alfvén oscillations coincides with that in formula (13) since $B_\varphi \ll B_z$.

Formula (13) is applied to diagnosing electric currents in flares. An example is furnished by the event on March 30, 2001 (Fig. 6) observed by Nobeyama Radio Observatory [31]. Analysis of quasiperiodic pulsations (at frequencies 0.001-0.005 Hz) has revealed an increase in current prior to the flare of up to 10^{10} A, and current dissipation during the

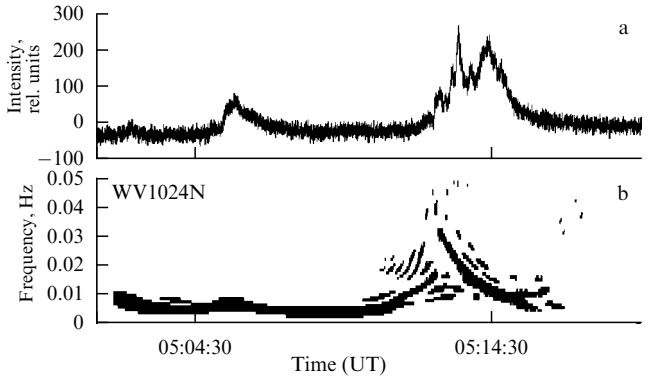

Figure 6. (a) The light curve for the event on 30.03.2001 as observed by spectropolarimeter Nobeyama at a frequency of 17.7 GHz. (b) The spectrum of low-frequency modulation of microwave emission obtained by Wigner–Wille method [32].

flare.

Another example is the solar flare on 24.03.1991 recorded by the Metsähovi Radio Observatory at a frequency of 37 GHz. The current decreased during the flare from 9×10^{11} A to 10^{11} A, the energy stored before the flare amounted to $W = LI^2/2 \sim 10^{32}$ erg, while the energy release power was $\mathrm{d}W/\mathrm{d}t \sim 10^{28}$ erg s^{-1} [29].

6. Parametric resonance

The excitation of acoustic oscillations in coronal magnetic loops may also occur through a parametric resonance with acoustic p-modes [29, 32]. It is known that the frequency of five-minute velocity oscillations of photospheric convection on the Sun (p-modes) is less than the cut-off frequency, i.e., they are reflected from the region of the temperature minimum. However, an analysis of observations of the Sun by the Metsähovi Radio Observatory at a frequency of 11.7 GHz revealed the presence of five-minute oscillations [32]. How do they penetrate into the corona? Moreover, two low-frequency signals with the periods of 3.3 and 10 min have been detected in the spectrum of oscillations, in addition to the signals with the five-minute period. The penetration of p-modes into the corona can be explained by the parametric excitation of acoustic oscillations in the coronal loops. Pulsations of photospheric convection velocity $|V_\mathrm{r}| = V_0 + V_\approx \sin \omega t$ modulate the EMF at the loop footpoints. As a result, the electric current $I_z = I_0 + I_\approx$ flowing in the loop is modulated, too. From the condition of tube radial equilibrium, it follows that the pressure in the tube also varies periodically with the amplitude $p_\approx = 4I_0 I_\approx/3\pi c^2 a^2$. As a result, the speed of sound appears to be periodically modulated:

$$c_\mathrm{s} = \left(\frac{\gamma k_\mathrm{B} T_0}{m_\mathrm{i}}\right)^{1/2}\left(1+\frac{\delta T}{T_0}\right) = c_{\mathrm{s}0}\left(1+\frac{2}{3}\,\frac{\gamma-1}{\gamma}\,\frac{I_0^2}{\pi c^2 a^2 p_0}\,\frac{I_\approx}{I_0}\cos\omega t\right), \qquad (14)$$

and the equation for the longitudinal plasma velocity in acoustic oscillations takes the form of the Mathieu equation, which describes the parametric instability [33]:

$$\frac{\mathrm{d}^2 V_z}{\mathrm{d}t^2} + \omega_0^2(1 + q\cos\omega t)V_z = 0\,, \qquad (15)$$

where the eigenfrequency of acoustic oscillations of the loop $\omega_0 = k_\parallel c_{\mathrm{s}0}$, $k_\parallel = s\pi/l$, $s = 1, 2, 3, \ldots$, $p_0 = 2nk_\mathrm{B}T_0$, $\gamma = c_p/c_v$, and the parameter $q = 4(\gamma-1)I_0 I_\approx/3\gamma\pi c^2 a^2 p_0$. The parametric instability develops in narrow zones near frequencies $\omega_n = n\omega/2$, $n = 1, 2, 3\ldots$. This implies that if the coronal loop is subjected to five-minute photospheric oscillations, acoustic oscillations with periods of 10 min (subharmonic), 5 min (pumping), and 3.3 min (the first upper frequency of parametric resonance) can be excited in the loop. By virtue of this mechanism, the energy of five-minute photospheric pulsations, which are reflected under normal conditions from the temperature minimum, penetrates into the corona, and may serve as an important heating source for the coronal plasma. Estimates in Ref. [34] have shown that heating of the solar corona exceeds radiative cooling, provided the current $I_0 > 7 \times 10^9$ A.

7. Diagnostics of magnetar coronae

One more illustration of the efficiency of methods utilized by coronal seismology is furnished by the diagnostics of coronae of magnetars — neutron stars with a radius of ~ 10 km, mass of $\sim 1.5 M_\odot$, and magnetic field $B \sim 10^{14} - 10^{15}$ G. The energy of the first pulse of an X-ray burst of a magnetar reaches 10^{46} erg [35], which is 14 orders of magnitude higher than the energy of the most powerful solar flares. The first pulse with a duration of about 1 s is followed by a 'pulsating tail' (frequencies from 20 to 2400 Hz) with a duration of about 200–400 s [36]. Existing models are not in the position to explain high Q factors of such pulsations: $Q \approx 10^5 - 10^7$. The magnetar corona comprising a hot plasma trapped by a magnetic field (trapped fireball), to which the pulsating tail is attributed, can be conceived of as a system of magnetic loops of various sizes with their electric current closed by the metallic core of the star [37]. The eigenfrequencies and Q factors of loops are expressed by the relationships $\omega = (LC)^{-1/2}$ and $Q = R^{-1}\sqrt{L/C}$, where $L = 2l\Lambda$ and $C \approx \varepsilon_\mathrm{A} S/l$, and the dielectric constant of the medium for Alfvén waves is $\varepsilon_\mathrm{A} = c^2/c_\mathrm{A}^2 \approx 1$, since from the dispersion relation $\omega_\mathrm{A} = k_\parallel c[1 + (4\pi\rho c^2/B^2)]^{-1/2}$ for Alfvén waves it follows that $c_\mathrm{A} \approx c$ in a magnetar corona.

Take as an example the diagnostics of SGR 1806-20 corona for the flare on December 27, 2004 [37]. The energy in the pulsating tail was on the order of 10^{44} erg. For a 'typical' loop assume that the energy stored in it reaches $\approx 2 \times 10^{43}$ erg. Assuming the loop length and radius are $l = 3 \times 10^6$ cm and $a = 3 \times 10^5$ cm, respectively, we find its inductance $L \approx 5 \times 10^6$ cm $= 5 \times 10^{-3}$ H. Supposing that a significant part of the energy stored in a typical loop ($W \approx 2 \times 10^{43}$ erg $= 2 \times 10^{36}$ J) has been released, we estimate the current $I = (2W/L)^{1/2} \approx 3 \times 10^{19}$ A. From the value of the current we estimate the magnitude of the φ-component of the loop magnetic field: $B_\varphi \approx I/ca \approx 10^{13}$ G. The concentration n of electron–positron pairs in the source is defined by the magnitude of current $I = encS$ and the cross section S of a coronal loop with the radius $a = 3 \times 10^5$ cm. For the current $I = 3 \times 10^{19}$ A, the quantity $n = 2 \times 10^{16}$ cm^{-3}, i.e., the Langmuir frequency $\nu_\mathrm{L} = 1.3 \times 10^{12}$ Hz falls in the terahertz band.

The power of energy release from a typical loop is $\mathrm{d}W/\mathrm{d}t \approx 2 \times 10^{40}$ erg s^{-1} $= 2 \times 10^{33}$ W. The magnitude of a loop resistance in the 'pulsating tail' is $R = (\mathrm{d}W/\mathrm{d}t)\, I^{-2} \approx \approx 2 \times 10^{-6}$ Ω. Such a resistance can be attributed to anomalous conductivity accompanying the excitation of small-scale plasma waves. The minimum (20 Hz) and maximum

(2400 Hz) pulsation frequencies of SGR 1806-20 allow one to estimate the capacitance of magnetic loops carrying the current. As a result, we obtain $C_1 \approx 1.5 \times 10^{-2}$ F and $C_2 \approx 8 \times 10^{-7}$ F, whereas the magnitudes of Q factors for minimum and maximum frequencies are $Q_1 \approx 3 \times 10^5$ and $Q_2 \approx 10^7$. Notice that the magnitude of the magnetic field found in this way, $B \approx 10^{13}$ G, is less than the quantum-electrodynamical threshold $B_{\rm QED} = 4.4 \times 10^{13}$ G at which the nonrelativistic Landau energy $\hbar eB/m_e c$ is comparable to the electron rest mass $m_e c^2$.

8. Conclusion

Natural manifestations of solar and stellar activity — oscillations and waves modulating the emission of the Sun and stars — contain information on coronal parameters, and often it is unique. As a consequence, coronal seismology offers an effective way of diagnosing stellar coronae. The variety of oscillatory and wave processes in solar and stellar coronae is not limited to the cases considered above. In this report, we did not touch on the seismologies of prominences and sunspots, which present separate branches of helioseismology. Further development in methods of coronal seismology is simulated by novel multiwavelength observations of the activity of the Sun and stars. Recent reviews of advances in coronal seismology [29, 38] need to be complemented even now. For instance, fresh SDO observations [39] have revealed manifestations of Kelvin–Helmholtz instability at the boundary of coronal plasma ejection.

This work was supported by RFBR grants 11-02-00103-a, 12-02-00616-a, and 12-02-92703-IND_a, by programs P-21 and P-22 of the Presidium of RAS, and also by Programs of Leading Scientific Schools NSh-1625.2012.2 and NSh-4185.2012.2.

References

1. Kosovichev A G, Duvall T L (Jr.), Scherrer P H *Solar Phys.* **192** 159 (2000)
2. Scherrer P H et al. *Solar Phys.* **275** 207 (2012)
3. Uchida Y *Publ. Astron. Soc. Jpn.* **22** 341 (1970)
4. Rosenberg H *Astron. Astrophys.* **9** 159 (1970)
5. Aschwanden M J et al. *Solar Phys.* **206** 99 (2002)
6. Zaitsev V V, Stepanov A V *Issled. Geomagn., Aeronomii Fiz. Solntsa* (37) 3 (1975)
7. Edwin P M, Roberts B *Solar Phys.* **88** 179 (1983)
8. Meerson B I, Sasorov P V, Stepanov A V *Solar Phys.* **58** 165 (1978)
9. Nakariakov V M, Melnikov V F, Reznikova V E *Astron. Astrophys.* **412** L7 (2003)
10. Nakariakov V M, Ofman L *Astron. Astrophys.* **372** L53 (2001)
11. Kopylova Yu G et al. *Pis'ma Astron. Zh.* **33** 792 (2007) [*Astron. Lett.* **33** 706 (2007)]
12. Tsap Y T et al. *Solar Phys.* **253** 161 (2008)
13. De Moortel I *Space Sci. Rev.* **149** 65 (2009)
14. McIntosh S W et al. *Nature* **475** 477 (2011)
15. Vasheghani Farahani S et al. *Astron. Astrophys.* **498** L29 (2009)
16. Nakariakov V M et al. *Astron. Astrophys.* **452** 343 (2006)
17. Zaitsev V V, Stepanov A V *Pis'ma Astron. Zh.* **8** 248 (1982) [*Sov. Astron. Lett.* **8** 132 (1982)]
18. Zaitsev V V, Stepanov A V *Pis'ma Astron. Zh.* **15** 154 (1989) [*Sov. Astron. Lett.* **15** 66 (1989)]
19. Braginskii S I, in *Voprosy Teorii Plazmy* (Reviews in Plasma Physics) Vol. 1 (Ed. M A Leontovich) (Moscow: Gosatomizdat, 1963) p. 183 [Translated into English (New York: Consultants Bureau, 1965) p. 205]
20. Priest E R *Solar Magneto-hydrodynamics* (Dordrecht: D. Reidel Publ. Co., 1982)
21. Stepanov A V et al. *Pis'ma Astron. Zh.* **31** 684 (2005) [*Astron. Lett.* **31** 612 (2005)]
22. Tsap Yu T et al. *Pis'ma Astron. Zh.* **37** 53 (2011) [*Astron. Lett.* **37** 49 (2011)]
23. Haisch B M, in *Activity in Red-Dwarf Stars*: *Proc. of the 71st Colloquium of the IAU, Catania, Italy, August 10–13, 1982* (Astrophysics and Space Science Library, Vol. 102, Eds P B Byrne, M Rodonò) (Dordrecht: D. Reidel Publ. Co., 1983) p. 255
24. Qin Z et al. *Solar Phys.* **163** 383 (1996)
25. Kopylova Yu G, Stepanov A V, Tsap Yu T *Pis'ma Astron. Zh.* **28** 870 (2002) [*Astron. Lett.* **28** 783 (2002)]
26. Spangler S R *Astrophys. J.* **670** 841 (2007)
27. Severny A *Space Sci. Rev.* **3** 451 (1964)
28. Alfvén H, Carlqvist P *Solar Phys.* **1** 220 (1967)
29. Zaitsev V V, Stepanov A V *Usp. Fiz. Nauk* **178** 1165 (2008) [*Phys. Usp.* **51** 1123 (2008)]
30. Zaitsev V V et al. *Astron. Astrophys.* **337** 887 (1998)
31. Zaitsev V V et al. *Izv. Vyssh. Uchebn. Zaved. Radiofiz.* **54** 243 (2011) [*Radiophys. Quantum Electron.* **54** 219 (2011)]
32. Kislyakova K G et al. *Astron. Zh.* **88** 303 (2011) [*Astron. Rep.* **55** 275 2011)]
33. Landau L D, Lifshitz E M *Mekhanika* (Mechanics) (Moscow: Fizmatgiz, 1958) [Translated into English (Oxford: Pergamon Press, 1960)]
34. Zaitsev V V, Kislyakova K G *Astron. Zh.* **87** 410 (2010) [*Astron. Rep.* **54** 367 (2010)]
35. Terasawa T et al. *Nature* **434** 1110 (2005)
36. Strohmayer T E, Watts A L *Astrophys. J.* **653** 593 (2006)
37. Stepanov A V, Zaitsev V V, Valtaoja E *Pis'ma Astron. Zh.* **37** 303 (2011) [*Astron. Lett.* **37** 276 (2011)]
38. Nakariakov V M, Erdélyi R (Guest Eds) "Solar coronal seismology" *Space Sci. Rev.* **149** (1–4) (2009)
39. Foullon C et al. *Astrophys. J.* **729** L8 (2011)

PACS numbers: **26.60.–c**, **67.10.–j**, 97.60.Jd
DOI: 10.3367/UFNe.0182.201209g.1006

Superfluid neutron stars

P S Shternin, D G Yakovlev

1. Cooling of neutron stars and properties of superdense matter

This talk summarizes the recent interpretation of observations (carried out in 2000–2010 with the NASA's Chandra X-ray orbital observatory) of the young (about 330-year old) neutron star in the Cassiopeia A supernova remnant. The data indicate that the neutron star has a carbon atmosphere and remains warm but shows noticeable cooling, so that its surface temperature has decreased by about 4% in the 10 years of observations. These are the first observations of an isolated neutron star cooling in real time. It is difficult to explain them using the cooling theory for nonsuperfluid neutron stars, but they are naturally explained if the superdense core of the star possesses a strong superfluidity of protons (with a critical temperature higher than 3×10^9 K) and a moderately strong superfluidity of neutrons (with the maximum critical temperature of order $(5-9) \times 10^8$ K over the stellar core). If the observations are correct, these data

P S Shternin, D G Yakovlev Ioffe Physical Technical Institute, Russian Academy of Sciences, St. Petersburg, Russian Federation;
St. Petersburg State Polytechnical University, St. Petersburg, Russian Federation
E-mail: pshternin@gmail.com, yak@astro.ioffe.rssi.ru

Uspekhi Fizicheskikh Nauk **182** (9) 1006–1012 (2012)
DOI: 10.3367/UFNr.0182.201209g.1006
Translated by D G Yakovlev; edited by A Radzig

give serious evidence of the presence of superfluidity in neutron star cores.

Typical masses of neutron stars are $M \sim 1.4\,M_\odot$ ($M_\odot$ is the mass of the Sun), and their radii are typically $R \sim 10-14$ km. Therefore, neutron stars are compact and contain superdense matter (see, e.g., Refs [1–3]). The mean density of the matter is a few times ρ_0, and the central density can exceed $(10-15)\,\rho_0$, where $\rho_0 = 2.8 \times 10^{14}$ g cm^{-3} is the saturation density of matter in atomic nuclei. Because of this high density, space–time around neutron stars is noticeably curved, and the notions of mass and radius become ambiguous (e.g., the baryon mass differs from the gravitational one [2]). In what follows, M means the gravitational mass, and R is the circumferential radius of the star. According to current theories, a neutron star has a relatively thin crust ($\lesssim 1$ km in thickness, and $\lesssim 0.01\,M_\odot$ in mass) and a bulky core, which extends from the density of $\rho \approx 0.5\,\rho_0$ to the stellar center and contains superdense nuclear matter. The stellar core is often divided into the outer core [$\rho \lesssim (2-3)\,\rho_0$], and the denser inner core. The outer core consists of close-packed neutrons, with an admixture of protons, electrons and muons, while the inner core may contain other particles, particularly, hyperons and free quarks. All fermions in the core are strongly degenerate; their typical Fermi energies run to a few hundred MeV. The properties of superdense matter are determined by strong interactions of nucleons and other particles (e.g., hyperons). The reliable theory of superdense matter is still absent because of difficulties in describing strong interactions and many-body effects in matter of supranuclear density; the experimental study of such matter in the laboratory is complicated.

One important aspect of the problem consists in superfluidity of superdense matter (see, e.g., Refs [2, 4, 5]). Nucleons, as well as hyperons and quarks, may form Cooper pairs and become superfluid under the action of the attractive component of strong interaction. In the inner crust of a neutron star, where free neutrons appear [1], these neutrons can undergo Cooper pairing in the spin-singlet state. However, near the core–crust interface the singlet-state attraction between neutrons is replaced by repulsion, and this superfluidity disappears. Nevertheless, triplet-state interaction may become attractive instead, so that the neutrons in the stellar core may be superfluid due to triplet-state Cooper pairing. Because the fraction of protons in the neutron star core is relatively small, protons can be superfluid due to singlet-state pairing. Since protons are electrically charged, their superfluidity also means superconductivity. Other strongly interacting particles (hyperons, quarks) can also be superfluid. At densities ρ much higher than ρ_0, the attractive component of interaction between any particles is reduced and any superfluidity disappears.

Microscopically, superfluidity creates a gap in the energy spectrum of particles near the Fermi level. In the case of singlet-state pairing, the gap is isotropic, while for triplet-state pairing it is anisotropic. The gap appears when the temperature falls below some critical temperature T_c; the gap grows with decreasing T and reaches a maximum at $T = 0$. Any superfluidity is specified by the particle pairing type and the critical temperature $T_c(\rho)$ which depends on density ρ. As mentioned above, in the nucleon stellar core one usually considers singlet-state superfluidity of protons and triplet-state superfluidity of neutrons, with the critical temperatures $T_{cp}(\rho)$ and $T_{cn}(\rho)$, respectively. Calculations of the critical temperatures strongly depend on the employed models of nuclear interaction and on methods to account for many-body effects. The theory predicts $T_{cn}, T_{cp} \lesssim 10^{10}$ K (with gaps $\lesssim 1$ MeV). Such superfluidity does not affect the equation of state of matter and neutron star structure but greatly modifies [6] the heat capacities, neutrino processes, kinetics, and hydrodynamics of superdense matter.

The nature of superdense matter remains an important unsolved problem of physics and astrophysics. It is being solved by comparing observations and theory of neutron stars in different ways (as described, e.g., in book [2]). Great progress has been attained in measuring the masses of neutron stars (radio pulsars) in compact binary systems. The recent reliable discovery [7] of the very massive radio pulsar J1614-2230, with a mass of $1.97 \pm 0.04\,M_\odot$, made unrealistic all theoretical models of soft and moderately stiff equations of state of neutron star matter. Such models had predicted that matter is rather soft, so that the maximum mass of stars is lower than the mass of the radio pulsar J1614-2230. Only stiff equations of state, which allow neutron stars to have such a mass, remained realistic. These results are in favor of nucleon models of superdense matter (see, e.g., Ref. [8]); they make models of matter containing other strongly interacting particles (hyperons or quarks) less probable, but do not fully reject these models. The unambigious solution to the problem of superdense matter should be obtained in the future.

Below, we discuss another method to explore superdense matter — by studying cooling of isolated neutron stars (see, e.g., papers [9–13] and references cited therein). Neutron stars are born hot (with an internal temperature of order 10^{11} K) in supernova explosions, but then gradually cool down. In about half a minute after its birth the star becomes fully transparent to neutrinos and cools down via powerful neutrino emission from the hot core. For about 10–200 years, the star is nonisothermal inside, but later it becomes isothermal; a strong temperature gradient remains only in a thin heat blanketing envelope near the surface. In 10^5-10^6 years, the neutrino emission weakens, and the star starts to cool mainly via thermal emission of photons from the surface. The theory gives cooling curves $T_s^\infty(t)$ — the dependence of the effective surface temperature of the star on its age t; the superscript ∞ means that the temperature is redshifted (for a distant observer). The star's cooling depends on the properties of superdense matter in the stellar core. Comparing theoretical curves $T_s^\infty(t)$ with measured surface temperatures of neutron stars of known ages allows one to explore superdense matter. The results have been reviewed in Refs [10–13].

The main cooling regulator of neutron stars with age $t \lesssim 10^5-10^6$ years is neutrino emission. For certainty, we restrict ourselves to neutron star models with nucleon cores. References to publications on cooling neutron stars with a more complicated nuclear composition can be found in review papers cited above. The main neutrino processes in stars with nucleon cores are listed in Table 1, where n denotes neutron, p proton, N nucleon (n or p), l electron or muon, and $\tilde{n}$ quasineutron (annihilating into a neutrino pair in the presence of superfluidity). Table 1 also presents order-of-magnitude estimates of neutrino luminosity L_ν due to these processes in a neutron star with internal temperature T; the notation $T_8 = T/10^8$ K was used. The three upper estimates are made neglecting superfluidity; the last estimate stands for a star with superfluid neutrons after the splash of neutrino emission which accompanies the onset of superfluidity (see Section 3).

Table 1. Neutrino luminosities L_ν for main reactions in nucleon cores of neutron stars.

Mechanism	Reaction	L_ν, erg s^{-1}
Direct Urca process	$n \to p l \bar{\nu}_l$, $p l \to n \nu_l$	$\sim 10^{40} T_8^6$
Modified Urca process	$nN \to pNl\bar{\nu}_l$, $pNl \to nN\nu_l$	$\sim 10^{32} T_8^8$
Nucleon collisions	$NN \to NN\nu\bar{\nu}$	$\sim (10^{30}-10^{31})\, T_8^8$
Cooper pairing of neutrons	$\tilde{n}\tilde{n} \to \nu\bar{\nu}$	$\lesssim (10^{33}-10^{34})\, T_8^8$

The standard (basic) neutrino mechanism involves the modified Urca process (the chain of two reactions listed in Table 1). In 10^5 years, it cools the star down to the temperature $T_s^\infty \sim 6 \times 10^5$ K. There are also weaker neutrino processes of neutrino-pair bremsstrahlung in nucleon collisions; they can be of three types — nn, np, and pp. In the inner core of a massive star with a nucleon core that has some specific equations of state, the much more powerful direct Urca process can operate [14] (a sequence of two reactions in Table 1), leading to fast cooling (to $T_s^\infty \sim 10^5$ K in 10^5 years). If such a process is allowed, massive stars cool down very quickly.

Superfluidity of nucleons strongly affects neutrino emission and heat capacity of the neutron star core, and hence its cooling (see Section 3). The effect of superfluidity has been taken into account for interpretation of the data for a long time but, because the critical temperatures $T_{cn}(\rho)$ and $T_{cp}(\rho)$ are actually unknown, the observations can be explained in many ways (see, e.g., Refs [10, 13]).

2. Neutron star in Cassiopeia A

Interest in cooling neutron stars noticeably grew in 2009–2010, after the publication of new results of X-ray data processing for observations of the cooling neutron star in the Cassiopeia A supernova remnant. The remnant is the brightest radio source in the Galaxy but weak in optics due to strong interstellar absorption. Its distance is estimated as $3.1^{+0.3}_{-0.1}$ kpc [15], and its age is reliably determined [16] as 330 ± 20 years from observations of the supernova remnant expansion. A compact stellar object (a neutron star or a black hole) created in the supernova explosion had been sought for a long time. However, the collapsar — the neutron star — was discovered in X-rays [17] only after the launch of the Chandra X-ray Orbital Observatory. The object has been observed for a long time [18–20]. The observed spectrum has been fitted by models of the black-body radiation, as well as by hydrogen and iron atmosphere models, but the inferred radius of the emission region has always been small (less than 5 km). These results implied emission from a hot spot on the stellar surface, but the radiation was not pulsating, whereas neutron stars usually spin rapidly producing noticeable pulsations.

The situation changed in 2009, when Ho and Heinke [21] published the results of their own interpretation of the same data with a carbon atmosphere model of the neutron star. They obtained the radius R of radiation region ranging $10-18$ km, compatible with the expected neutron star radius. The inferred stellar mass $M = (1.5-2.4)\, M_\odot$ fell also in the range of expected neutron star masses. According to their interpretation, the magnetic field in the neutron star atmosphere, $B \lesssim 10^{11}$ G, is insufficiently strong to produce noticeable pulsations of the radiation of the spinning star. The inferred surface temperature was $T_s^\infty \sim 1.5 \times 10^6$ K, in good agreement [22] with the standard cooling of a (nonsuperfluid) neutron star via neutrino emission due to the modified Urca process. This is the youngest neutron star whose surface thermal emission has been detected. Unfortunately, its temperature T_s^∞ was in good agreement with the standard theory, which did not make the results very interesting.

However, the next paper by Heinke and Ho [23] became sensational. The authors reprocessed the same data by ordering them in time and determining the temperature T_s^∞ as a function of time t. It appeared that in 9 years of observations the temperature had dropped by 4% (Fig. 1), and the thermal flux dropped by 21%. The next observations performed in November 2010 [24] confirmed these results. If they are correct, they are the first observations of a cooling isolated neutron star in real time, and this cooling is extremely 'fast' from a theoretical point of view. Formally, it is convenient to introduce the temperature drop rate as

$$s = -\frac{\mathrm{d} \ln T_s^\infty}{\mathrm{d} \ln t}\,, \qquad (1)$$

which, in our case, is $s \approx 1.35 \pm 0.15$ (here, we present 1σ error bars, while in Fig. 2 we give 2σ error bars). Had the star cooling via neutrino emission been due to the direct or modified Urca process, we would have had $s \sim 0.1$ (see the dashed line in Fig. 2), and the T_s^∞ decline in 10 years would have been unnoticeable. A sharp drop in T_s^∞ occurs in a young neutron star (10–200 years old) at the end of internal thermal relaxation [25–27], but the thermal relaxation of the given star should have been over. In other words, the neutron star is sufficiently warm but cannot be described by the ordinary cooling theory for nonsuperfluid neutron stars.

3. Cooling of superfluid neutron stars

Observations of the neutron star in Cassiopeia A are naturally explained [24, 29] by the cooling theory of superfluid neutron stars. The theory was formulated in its final form in 2004 [28, 30].

We illustrate the cooling calculations following Ref. [24]. The computations have been performed with the equation of state of nucleon matter in the neutron star core suggested by Akmal, Pandharipande, and Ravenhall [31]. Specifically, we have used the parametrization of their results [31] derived in Ref. [32] and denoted as APR I in Ref. [33]. For this equation of state, the maximum mass of stable neutron stars is $M_{max} = 1.929\, M_\odot$; the powerful direct Urca process becomes open in stars with $M > 1.829\, M_\odot$. The calculations have been mostly performed for the $1.65\, M_\odot$ star. The central density of such a star is shown by the vertical dotted line in Fig. 1a. The dashed line N in Fig. 1b describes the cooling of this star, neglecting the superfluidity effects.[1] One can see that it cannot provide the required steep slope of the cooling curve. In the inset to Fig. 1b, which is drawn on a smaller scale, one

[1] In the main panel of Fig. 1b, in contrast to the inset, the curve N is slightly raised, in order to fit the figure and demonstrate its insufficiently steep slope.

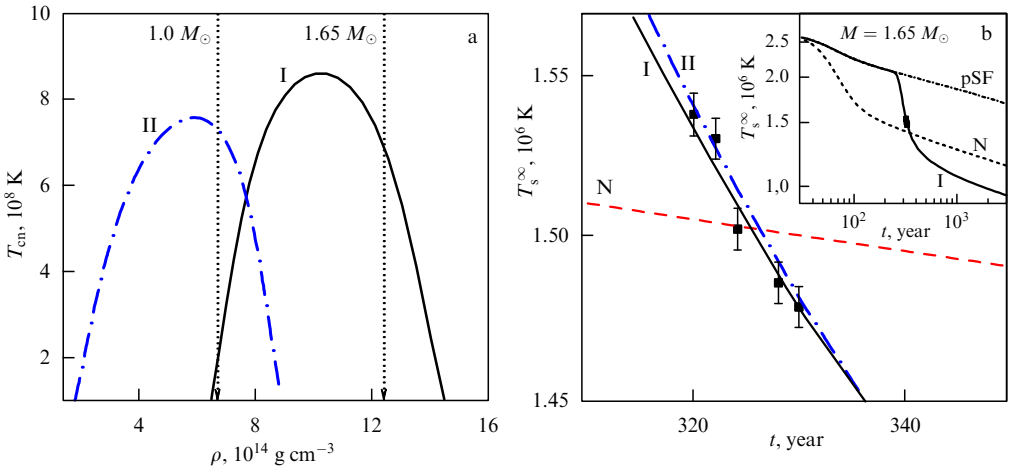

Figure 1. (a) Two models I and II for the critical temperature T_{cn} of triplet-state pairing of neutrons as a function of density ρ in a neutron star core. Vertical dotted straight lines show the central densities of stars of masses $M = 1.0\,M_\odot$ and $1.65\,M_\odot$. (b) Decline in the surface temperature T_s^∞ of the Cassiopeia A neutron star with time t. Dots with error bars are observational data. Curve N depicts a typical cooling curve for a nonsuperfluid star. Curves I and II are theoretical cooling curves for the $1.65\,M_\odot$ star, whose core contains strongly superfluid protons and neutrons with type I and II superfluidity, respectively. The inset shows curves I and N on a smaller scale and also curve pSF for a star with strongly superfluid protons and normal neutrons in the core.

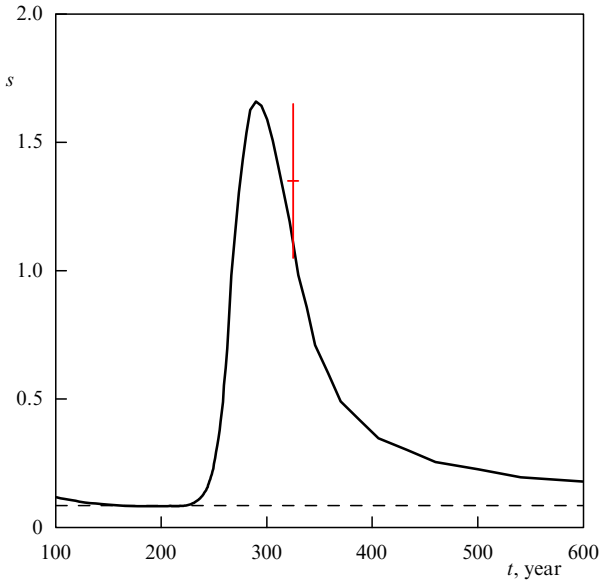

Figure 2. Solid line displays the slope s of the theoretical cooling curve for a $1.65\,M_\odot$ neutron star with strong proton superfluidity and type I neutron superfluidity (see Fig. 1), as compared with the observational data (with 2σ error bars) for the neutron star in Cassiopeia A. Dashed line reproduces $s(t)$ for a nonsuperfluid star (curve N in Fig. 1).

can well observe the desirable steep slope of curve N, but in the earlier epoch ($t \lesssim 100$ yr). It manifests the end of the inner thermal relaxation of the star, which cannot be used to explain the observations because it is difficult to delay the relaxation to the current epoch of $t \approx 330$ years.

More important for us would be the effect of superfluidity on neutrino processes in the stellar core. Because neutrino emission is generated in reactions involving strongly degenerate nucleons, the main contribution to this emission is provided by nucleons with energies near the Fermi level. Superfluidity of nucleons suppresses all the reactions involving these nucleons because of the appearance of a gap in their energy spectrum. When the temperature T falls much below T_c, the suppression becomes exponentially strong (see, e.g., Ref. [5]).

In addition to suppressing standard neutrino processes, superfluidity opens a specific mechanism of neutrino pair emission due to Cooper pairing of nucleons [34]. It can be treated as annihilation of quasiparticles producing neutrino pairs (see Table 1). The process is kinematically allowed owing to a distortion of the nucleon energy spectrum by the gap when T falls below T_c. Its intensity first strongly increases, reaches a maximum at $T \approx 0.8\,T_c$, and then exponentially declines with decreasing T (again, because of a gap occurrence). It is a rare neutrino process whose intensity can increase with decreasing T. The process is strongly affected by many-body (collective) effects, which was first pointed out by Leinson [35] and later studied in a number of papers (see, e.g., Refs [36–41] and references cited therein, as well as a discussion in review [12]). An account for collective effects is complicated (model-dependent), and the results are rather controversial.

In the nucleon core of the neutron star one can expect neutrino emission due to singlet-state Cooper pairing of protons and triplet-state Cooper pairing of neutrons (see Section 1). However, the emission due to pairing of protons is strongly suppressed by the smallness of reaction rate constants (see, e.g., Ref. [6]). It can be additionally reduced by many-body effects. Similar collective effects can strongly suppress neutrino emission due to singlet-state Cooper pairing of neutrons in the inner star's crust, but this emission, even nonsuppressed, is integrally weak due to the small volume of the crust, thus weakly affecting neutron star cooling. The second process of the given type in the stellar core is associated with neutrino emission due to triplet-state pairing of neutrons. Such emission can be sufficiently intense; it can be suppressed by collective effects, but much weaker than suppression due to singlet-state pairing (see, e.g., Ref. [41]). This process is important, and it will be considered below. Its neutrino luminosity is determined by integrating the neutrino emissivity over the region of triplet-state superfluidity of neutrons in the core (see, e.g., Ref. [30]). The latter region is determined by the critical temperature profile $T_{cn}(\rho)$

and by the current core temperature; the region widens when the star cools. The maximum of $T_{\rm cn}(\rho)$ specifies the moment when this neutrino emission starts. The width of the $T_{\rm cn}(\rho)$ profile regulates the intensity of the neutrino outburst and the subsequent efficiency of this neutrino emission in the star. According to computations, the neutrino luminosity due to Cooper pairing of neutrons can be 30–100 times larger than the luminosity due to the modified Urca process in a nonsuperfluid star. This can noticeably accelerate cooling in comparison with the standard one, as reflected in Table 1.

Thus, singlet-state proton superfluidity only suppresses neutrino luminosity of the stellar core, while triplet-state neutron superfluidity can strongly enhance this luminosity.

4. Superfluidity of the neutron star in Cassiopeia A

The theory should explain two apparently contradictory observational facts (see Section 2): the high temperature ($T_{\rm s}^{\infty} \approx 1.5 \times 10^6$ K) and fast cooling rate ($s \approx 1.3$) of the star. With this rate, the star should have been much colder than it is. These facts can be naturally explained [24, 29] assuming the presence of strong singlet-state proton superfluidity and moderately strong triplet-state neutron superfluidity in the stellar core. The cooling theory allows one to choose such $T_{\rm cn}(\rho)$ and $T_{\rm cp}(\rho)$ profiles in the core, which lead to the observed values of $T_{\rm s}^{\infty}$ and s.

Numerical simulations show that the $T_{\rm cn}(\rho)$ profile should have a wide peak with the maximum $T_{\rm cn}^{\rm max}(\rho) \sim (5-9) \times 10^8$ K. The maximum height guarantees that neutron superfluidity in the core appeared only a few decades ago; the neutrino emission due to Cooper pairing of neutrons gained its full strength, but had no time to greatly cool the star. By way of illustration, Fig. 1a gives two phenomenological $T_{\rm cn}(\rho)$ profiles (curves I and II); their effect on cooling is explained below. The profiles are taken from Ref. [24], where curve I is denoted as (a), and curve II as (c).

To explain the observational data, we also need proton superfluidity. It has to be strong, with the critical temperature $T_{\rm cp}(\rho) \gtrsim 3 \times 10^9$ K in the stellar core. The specific density dependence of $T_{\rm cp}$ is unimportant here. Such superfluidity appears early ($t \lesssim 1$ year) and suppresses all basic neutrino processes involving protons: Urca processes (modified or even direct ones), and neutrino-pair bremsstrahlung due to nucleon–proton collisions. It is only a relatively weak neutrino-pair generation process due to neutron–neutron collisions that survives (before the onset of neutron superfluidity). Hence, the neutrino luminosity of a star with normal neutrons is low, and the star remains noticeably hotter than in the course of the standard cooling due to the modified Urca process. The corresponding cooling curve (curve pSF) is plotted in the inset to Fig. 1b, only in this case the subsequent neutrino outburst due to Cooper pairing of neutrons gives the high observable cooling rate. As seen from Fig. 1, both models I and II for neutron superfluidity in a $1.65\,M_{\odot}$ star agree with the observations of the neutron star in Cassiopeia A, with model I being slightly better.

Moreover, according to Ref. [24], in the wide range of masses from $1.3\,M_{\odot}$ to $1.9\,M_{\odot}$ one can choose such a $T_{\rm cn}(\rho)$ profile in the stellar core, which explains the observations. For $M \gtrsim 1.5\,M_{\odot}$, these profiles are only slightly different, while the maximum $T_{\rm cn}^{\rm max}$ at lower M should be somewhat higher and shifted towards lower ρ. Theoretical results are also sensitive [24] to poorly studied collective effects on the neutrino emission due to Cooper pairing of neutrons in dense matter (see above).

It is important that the theory predicts a nontrivial behavior of the cooling rate (factor s, see Fig. 2). When the star reaches the state of internal thermal relaxation, the theory gives the standard value of $s \sim 0.1$. However, after the onset of neutron superfluidity, s jumps by a factor of a few tens, reaches a maximum, and then declines to its standard level $s \sim 0.1$. A noticeable rise in s above its standard value is the evidence of neutrino outburst within the star; it does not last very long and indicates a special period in the star's life. One can show that an accurate measurement of $s(t)$ would allow one to infer the most important parameter — the neutrino cooling function (ratio of neutrino luminosity and heat capacity of the star) within that period. It could give very useful information on the internal structure of the neutron star: first and foremost, on the critical temperature profile $T_{\rm cn}(\rho)$ for neutron superfluidity. It seems that the present observations of the neutron star in Cassiopeia A are being made at this very period, but the factor s is measured with large uncertainty. Clearly, to observe the star in this period is a matter of good luck. If the proposed scenario is correct, s should noticeably decline over tens of years, which can be checked in future observations.

5. Cassiopeia A and other cooling neutron stars

At the next stage, it is useful to analyze our results in combination with the data on other cooling neutron stars [24]. It is reasonable to assume that the properties of superdense matter (most importantly, the equation of state) are the same in all neutron stars, but stars have different masses (central densities), rotation periods, magnetic fields, chemical compositions of surface layers, etc. In this case, the $T_{\rm cn}(\rho)$ and $T_{\rm cp}(\rho)$ profiles are the same in all stars (although they extend to different central densities).

For our analysis, we have taken [24] stellar models with the same APR I equation of state. We have calculated the cooling curves for stars of various masses with different $T_{\rm cn}(\rho)$ and $T_{\rm cp}(\rho)$; the results have been compared with the observations of all cooling neutron stars whose $T_{\rm s}^{\infty}$ and t have been measured (estimated). Observational data on these stars have been taken from the sources cited in Ref. [24]. The results for strong proton superfluidity and type I or II neutron superfluidity are presented in Fig. 3. Shaded are those ranges of $T_{\rm s}^{\infty}$ which are filled by the cooling curves for neutron stars of various masses (from $1\,M_{\odot}$ to $1.929\,M_{\odot}$). The upper curves on both panels refer to the $1\,M_{\odot}$ star; this star shows the slowest cooling in our model. The lower curve refers to the most massive $1.929\,M_{\odot}$ star representing the fastest cooler. For simplicity, we assume that the powerful direct Urca process of neutrino emission in massive stars is formally allowed but fully suppressed by strong proton superfluidity. If this were not so, massive stars would cool much faster, and the shaded regions in Fig. 3 would drop to much lower temperatures [24]. In addition to the cooling curves for the $1\,M_{\odot}$ and $1.929\,M_{\odot}$ stars, we also plotted the intermediate curves for $1.65\,M_{\odot}$ stars.

As follows from Fig. 1, in model II for neutron superfluidity stars of all masses undergo the stage of neutrino outburst after the onset of neutron superfluidity. It is seen, however, from Fig. 3b that such models for neutron superfluidity contradict observations. These models are good for explaining the coldest neutron stars (for their ages), like the Vela pulsar. However, they cannot explain the warmest middle-aged stars, for instance, PSR 0656+14 — after the neutrino outburst it would have been much colder than

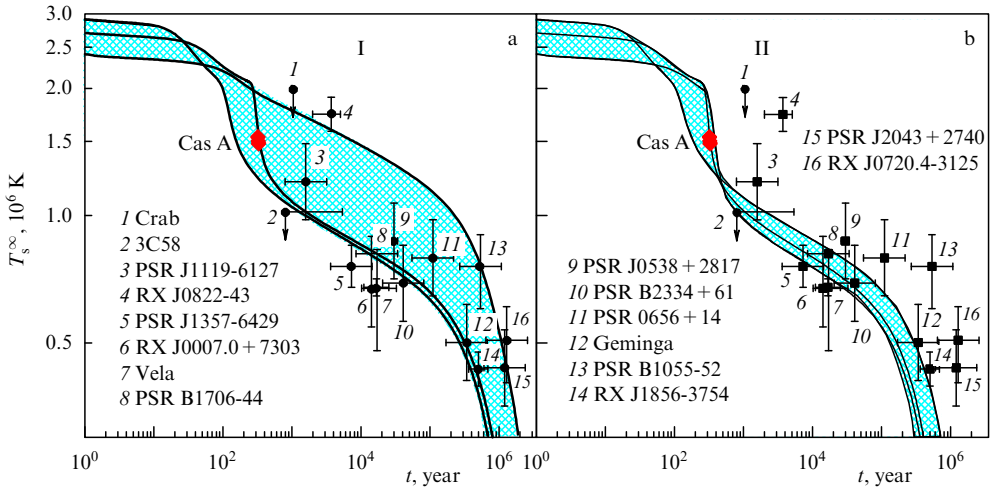

Figure 3. Observational data on cooling neutron stars as compared with theoretical cooling curves for neutron stars of different masses possessing strong superfluidity of protons and type I (a) or II (b) superfluidity of neutrons. Shaded regions are filled by cooling curves of stars of various masses, from $M = M_\odot$ (upper curves) to $\approx 2\,M_\odot$ (lower curves). As an example, the solid lines show cooling of a $1.65\,M_\odot$ star. Superfluidity I can explain the observations of all stars, while superfluidity II cannot.

required. The observations of all stars can be explained only by the bell-shaped $T_{\rm cn}(\rho)$ profile shifted to the inner core of a neutron star, like the type I profile (Fig. 3a). In that case, neutron superfluidity either does not appear at all in a low-mass star or appears too late, when it does not affect the cooling. In more massive stars, it appears earlier and initiates noticeable cooling. A similar $T_{\rm cn}(\rho)$ profile was suggested earlier [30] for explaining the data available at that time. Surprisingly, it also explains the observations of the Cassiopeia A neutron star. Observations of all stars restrict the $T_{\rm cn}(\rho)$ profile rather strongly [30]; the neutron star in Cassiopeia A should not be too light, $M \gtrsim 1.4\,M_\odot$, and the masses of other stars should be ranged. For instance, the Vela pulsar should be massive, and the PSR 0656+14 should have a low mass. Let us stress that the given $T_{\rm cn}(\rho)$ profile does not agree with many microscopic calculations (which indicate that triplet-state pairing occurs at lower densities), but it is not excluded by such numerical simulations (see papers [30, 42] and references cited therein). To avoid this nonstandard $T_{\rm cn}(\rho)$ dependence, we can assume that the $T_{\rm cn}(\rho)$ profile is wide (more standard) and extends to the outer stellar core, but the efficiency of neutrino emission due to Cooper pairing of neutrons at lower densities is strongly suppressed (for instance, by collective effects). Then the neutrino emissivity profile in the core will be similar to that for type I superfluidity.

6. Conclusions

We have discussed recent results obtained by Ho and Heinke [21, 23], who processed 10-year long spectral observations of the young cooling neutron star in the Cassiopeia A supernova remnant using the Chandra X-ray orbital observatory. The results reveal an extraordinarily fast (according to theoretical standards) cooling of the warm star, which is not described by the cooling theory of nonsuperfluid stars. We show that it is easily explained provided the star's core possesses strong singlet-state superfluidity of protons (which suppresses neutrino emission and slows down the cooling just after the star's birth) and moderately strong triplet-state superfluidity of neutrons (which appeared a few decades ago and produced a strong neutrino outburst that is accelerating the cooling in the present epoch). If this explanation is correct, this is the first serious evidence for the presence of superfluidity in neutron star cores that comes from observations of cooling neutron stars. Before these results, the main observational manifestation of superfluidity was thought to be provided by pulsar glitches — sudden changes in pulsar spin periods (see, e.g., Ch. 1 in monograph [2] and references cited therein).

The neutrino outburst triggered by the onset of neutron superfluidity in the Cassiopeia A neutron star should be followed by a rapid decrease in $s(t)$, which can be checked in a few decades of future observations. We stress that the explanation of the data was proposed independently in two publications [24, 29], which differ only in details. It is based on the theory that, in turn, was devised independently in two publications [28, 30] by the same teams.

Two alternative explanations have been suggested for the neutron star phenomenon in Cassiopeia A. The first one [43] assumes that the young neutron star was born rapidly spinning, with its central density very close to the critical density at which the direct Urca process starts (if not suppressed by superfluidity). Then, according to the authors, the star slows down by the pulsar braking mechanism, its central density increases, and the direct Urca process comes into play, triggering powerful neutrino emission and observed rapid cooling. This explanation is, in principle, valid, but its realization is highly improbable (it requires the finest tuning of parameters). The second explanation [44] is based on the nonstandard model of thermal insulation of the neutron star, which allows the authors to delay the thermal relaxation till the present epoch. The observed sharp drop in the surface temperature of the star is explained by the cessation of the thermal relaxation. This model of thermal insulation cannot be justified and contradicts well-known reliable models (see, e.g., Refs [45–47]).

Returning to our primary interpretation, we notice that it allows us to explain observations of cooling of all isolated neutron stars by one and the same model for nucleon superfluidity in the stellar core. Moreover, an analogous model was suggested much earlier to explain the data on cooling neutron stars available at that time [30]. The new data on the neutron star in Cassiopeia A surprisingly support the

old results. Sceptics can disagree with the suggested interpretation but may treat it as a hint of how neutrino emissivity within the neutron star should behave to explain the data. In any case, the suggested interpretation of observations of the neutron star in Cassiopeia A is preliminary and has to be confirmed. First, the assumed neutrino outburst is a rare event; it is a surprise that its consequences are being observed. Second, the region of triplet-state pairing of neutrons is shifted too deeply into the star's core, in contrast to the majority of microscopic calculations. Third, the ageing of the X-ray detectors of the Chandra observatory may lead to errors in their calibration and data processing [48]. However, the interest in the neutron star in Cassiopeia A is high, and we hope the situation with observations and theoretical interpretation will be clarified in the near future.

The work was supported by the RFBR (grants 11-02-00253-a and 11-02-12082-ofi-m-2011), RF Presidential Program NSh-4035.2012.2, Ministry of Science and Education of the Russian Federation (contract 11.G34.31.0001), and the Dynasty Foundation.

References

1. Shapiro S L, Teukolsky S A *Black Holes, White Dwarfs, and Neutron Stars* (New York: Wiley, 1983) [Translated into Russian (Moscow: Mir, 1985)]
2. Haensel P, Potekhin A Y, Yakovlev D G *Neutron Stars 1*: *Equation of State and Structure* (New York: Springer, 2007)
3. Lattimer J M, Prakash M *Phys. Rep.* **442** 109 (2007)
4. Lombardo U, Schulze H-J *Lecture Notes Phys.* **578** 30 (2001)
5. Yakovlev D G, Levenfish K P, Shibanov Yu A *Usp. Fiz. Nauk* **169** 825 (1999) [*Phys. Usp.* **42** 737 (1999)]
6. Yakovlev D G et al. *Phys. Rep.* **354** 1 (2001)
7. Demorest P B et al. *Nature* **467** 1081 (2010)
8. Lattimer J, Prakash M, in *From Nuclei to Stars* (Ed. S Lee) (Singapore: World Scientific, 2011) p. 275
9. Pethick C J *Rev. Mod. Phys.* **64** 1133 (1992)
10. Yakovlev D G, Pethick C J *Annu. Rev. Astron. Astrophys.* **42** 169 (2004)
11. Page D, Geppert U, Weber F *Nucl. Phys. A* **777** 497 (2006)
12. Page D et al. *Astrophys. J.* **707** 1131 (2009)
13. Yakovlev D G et al. *AIP Conf. Proc.* **983** 379 (2008)
14. Lattimer J M et al. *Phys. Rev. Lett.* **66** 2701 (1991)
15. Reed J E et al. *Astrophys. J.* **440** 706 (1995)
16. Fesen R A et al. *Astrophys. J.* **645** 283 (2006)
17. Tananbaum H *IAU Circ.* (7246) 1 (1999)
18. Pavlov G G et al. *Astrophys. J.* **531** L53 (2000)
19. Chakrabarty D et al. *Astrophys. J.* **548** 800 (2001)
20. Pavlov G G, Luna G J M *Astrophys. J.* **703** 910 (2009)
21. Ho W C G, Heinke C O *Nature* **462** 71 (2009)
22. Yakovlev D G et al. *Mon. Not. R. Astron. Soc.* **411** 1977 (2011)
23. Heinke C O, Ho W C G *Astrophys. J.* **719** L167 (2010)
24. Shternin P S et al. *Mon. Not. R. Astron. Soc.* **412** L108 (2011)
25. Nomoto K, Tsuruta S *Astrophys. J.* **312** 711 (1987)
26. Lattimer J M et al. *Astrophys. J.* **425** 802 (1994)
27. Gnedin O Y, Yakovlev D G, Potekhin A Y *Mon. Not. R. Astron. Soc.* **324** 725 (2001)
28. Page D et al. *Astrophys. J. Suppl.* **155** 623 (2004)
29. Page D et al. *Phys. Rev. Lett.* **106** 081101 (2011)
30. Gusakov M E et al. *Astron. Astrophys.* **423** 1063 (2004)
31. Akmal A, Pandharipande V R, Ravenhall D G *Phys. Rev. C* **58** 1804 (1998)
32. Heiselberg H, Hjorth-Jensen M *Astrophys. J.* **525** L45 (1999)
33. Gusakov M E et al. *Mon. Not. R. Astron. Soc.* **363** 555 (2005)
34. Flowers E, Ruderman M, Sutherland P *Astrophys. J.* **205** 541 (1976)
35. Leinson L B *Nucl. Phys. A* **687** 489 (2001)
36. Leinson L B, Pérez A *Phys. Lett. B* **638** 114 (2006)
37. Sedrakian A, Müther H, Schuck P *Phys. Rev. C* **76** 055805 (2007)
38. Kolomeitsev E E, Voskresensky D N *Phys. Rev. C* **77** 065808 (2008)
39. Leinson L B *Phys. Rev. C* **78** 015502 (2008)
40. Steiner A W, Reddy S *Phys. Rev. C* **79** 015802 (2009)
41. Leinson L B *Phys. Rev. C* **81** 025501 (2010)
42. Kaminker A D et al. *Mon. Not. R. Astron. Soc.* **365** 1300 (2006)
43. Negreiros R, Schramm S, Weber F *Phys. Rev. D* **85** 104019 (2012); arXiv:1201.2381
44. Blaschke D et al. *Phys. Rev. C* **85** 022802(R) (2012)
45. Gudmundsson E H, Pethick C J, Epstein R I *Astrophys. J.* **272** 286 (1983)
46. Potekhin A Y, Chabrier G, Yakovlev D G *Astron. Astrophys.* **323** 415 (1997)
47. Potekhin A Y et al. *Astrophys. J.* **594** 404 (2003)
48. Weisskopf M C et al. *Astrophys. J.* **743** 139 (2011)